ADVANCED MATERIALS TECHNOLOGIES
www.advmattechnol.de

Toward Fully Printed Soft Actuators: UV-Assisted Printing of Liquid Crystal Elastomers and Biphasic Liquid Metal Conductors

*João Sgotti Veiga, Manuel Reis Carneiro, Rafael Molter, Michael Vinciguerra, Lining Yao, Carmel Majidi, and Mahmoud Tavakoli**

Development of soft and compliant actuators has attracted tremendous attention due to their use in soft robotics, wearables, haptics, and assistive devices. Despite decades of progress, the goal of entirely digitally-printed actuators has yet to be fully demonstrated. Digital printing permits rapid customization of the actuator's geometry, size, and deformation profile, and is a step toward mass customization of user-specific wearables and soft robotic systems. here, a set of materials and methods are demonstrated for rapid fabrication of 3D-printed Liquid Crystal Elastomer actuators electrically stimulated via a printed joule heater composed of a Liquid Metal (LM)-filled elastomer composite. Unlike other Ag-based inks, this LM-elastomer composite is sinter-free, enabling room-temperature printing, and is stretchable, allowing cyclic actuation without electrical or mechanical failure of the conductor. By optimizing printing parameters, and improving the photo-polymerization setup, a printed actuator that bends to an angle of 320° is demonstrated, with lower power consumption than previous LCE actuators. We also demonstrate a customized UV-polymerization setup that permits photo-curing of the LCE actuator in ≈90s, i.e., >500x faster compared to previous works. The rapid photo-polymerization enables progress toward 3D-printing of multi-layer actuators and is a step toward mass customization of fully digitally-printed robotic and wearable devices.

1. Introduction

Progress in soft robotics, wearable assistive and rehabilitation devices, and compliant human machine interfaces for virtual reality depends on novel forms of soft actuators that can replace the bulky motors used in traditional robotic systems.[1] There are a variety of emerging actuator technologies, including piezoelectric actuators,[2–6] pneumatic artificial muscle,[7–14] dielectric elastomer actuators,[15–17] shape memory alloys,[18–21] and shape memory polymers.[22–24] Recently, liquid crystal elastomers (LCE) actuators have drawn attention[25–33] mainly due to two promising advantages: the simple synthesis of the polymer itself and the fact that it can be printed and patterned through digital means.[29,25–27,34] LCE actuation relies on the transition between two crystalline phases: ordered alignment of mesogens along a single axis (nematic state) and a disordered (isotropic) phase.[35] This transition can be induced by heat, and results in macroscopic contraction of the transducer along the axis of nematic alignment. LCEs are promising materials for "4D printing" [30,31,36] as they can be patterned through extrusion-based printing techniques commonly used in 3D printing and direct ink writing of structures that can undergo reversible shape change. In addition, one of the challenges in the fabrication of LCE actuators – the alignment of mesogens[37] – is automatically addressed through the shear-induced stresses generated in extrusion tips,[38] which align the mesogens in the same direction, leading to improved actuation.[30,39] While optical and thermal-induced actuation have been shown in several works,[40,41] for digitally controllable devices, electrically-stimulated LCE actuators are preferred since they can be directly compatible with standard robotic controllers and power electronics. Therefore, in some works, a Joule heater has been utilized to control the shape change of LCE actuators.[29,42]

Despite progress in 4D printing of LCE-based structures, challenges remain in creating electrically-responsive LCE actuators using entirely digital printing techniques. Progress in the use of LCEs as actuators in emerging applications relies on new method to digitally print all components of the actuator with the desired shape and geometry, with the ultimate goal of enabling mass

J. Sgotti Veiga, M. Reis Carneiro, R. Molter, M. Tavakoli
Institute of Systems and Robotics
Department of Electrical and Computer Engineering
University of Coimbra
Coimbra 3030–290, Portugal
E-mail: mahmoud@isr.uc.pt

M. Reis Carneiro, M. Vinciguerra, C. Majidi
Soft Machines Lab
Department of Mechanical Engineering
Carnegie Mellon University
Pittsburgh, PA 15213, USA

M. Vinciguerra, L. Yao
Morphing Matter Lab
Human-Computer Interaction Institute
Carnegie Mellon University
Pittsburgh, PA 15213, USA

The ORCID identification number(s) for the author(s) of this article can be found under https://doi.org/10.1002/admt.202300144

DOI: 10.1002/admt.202300144

customization of custom technologies. When it comes to LCE actuators, such objectives require addressing specific technical challenges. First, successful digital fabrication requires extrusion printing of both the LCE and soft conductors that can function as the soft Joule heater. Second, since the actuators are subject to repeated mechanical strain during actuation, the printed conductor must be stretchable in order to withstand repetitive deformation. Most existing printable conductive inks suffer from having an increased electrical resistance over cycles, which ultimately results in electrical failure. Moreover, the need for thermal sintering of common conductive inks at temperatures usually above 100 °C results in warping and deformation of the underlying printed LCEs. Third, the current curing (i.e., UV-crosslinking) time for LCE actuators is several hours in most published works.[43–46] An improvement was made in,[36] in which the authors state a curing time of 5 min, which can be attributed to the use of RM82 liquid crystal monomer which has lower crosslinking density than the commonly used RM257 thanks to its single acrylate group which can limit its strength and thermal stability, leading to a weaker LC polymer network.' Such prolonged curing time is an obstacle for 3D printing and rapid prototyping of complex, multilayer geometries which becomes more of a problem as the UV assisted polymerization process is not very effective on thicker structures.

Liquid metal has been a commonly used approach to address the low strain tolerance of conventional electronic conductors and has been implemented as Joule heaters.[41,47,48] Eutectic Gallium Indium (EGaIn) is a popular LM alloy that can maintain high electrical conductivity when subject to mechanical strain, meaning that they can be reliably used as both heating unit and electrical interconnects required for activating individual LCE actuators. Nevertheless, digital printing of liquid metals is challenging due to its low viscosity and high surface tension.[49] Therefore, in previous works, liquid metal was either used as a coat [40]for LCE fibers or as a core material.[50] Nevertheless, even when printed through well-established manual techniques such as stencil deposition, the smearing behavior of the liquid metal is an obstacle against reliable long-term usability of the actuators.[16]

In this work, we demonstrate a fully digitally printed LCE based actuator, with a Joule heater based on a EGaIn-Ag-SIS composite that we recently demonstrated in ref. [51] This biphasic conductive composite combines stretchable and non-smearing behavior and permits direct digital printing of the conductive heater and interconnects at room temperature. Furthermore, we study how some printing parameters – number of stacked layers and diameter of extrusion nozzle affect the actuation efficiency of printed LCE transducers. Finally, we implement a customized UV curing chamber with a wavelength that matches the peak absorption of the radical photoinitiator used in LCE composite. This UV chamber is designed for illuminating both sides of the LCE leading to a homogeneous curing of the whole LCE surface area. We show that using this device it is possible to significantly reduce the polymerization time from several hours [43–46] to ≈90 s. As a result of these improvements, we demonstrated a fully digitally printed LCE actuator with printed Joule heater that can curl around itself to an unprecedented angle of 320° with a modest power consumption of ≈620 mW cm^{-2}, thereby showing significant improvement over previous work.[43]

2. Results and Discussion

2.1. Materials Synthesis and Actuator Fabrication

The liquid crystal elastomer (LCE) is obtained by mixing a liquid crystal monomer (RM257) with a chain extender (n-Butylamine) and a photoinitiator (Irgacure 369, I369) in a planetary mixer, as shown in **Figure 1**A. The vial containing the LCE solution is covered with a UV blocking film and placed in a hot bath at 85 °C for 75 min. The full synthesis process is detailed in the Experimental Section. The LCE paste is then transferred to a metallic extrusion barrel (stainless steel tubes, 20cc – Hyrel 3D) and loaded into the ink dispensing system (Multi-tool 3D printer, Hydra21 – Hyrel 3D), followed by a UV flashlight (Alonefire, ≈3600 mW cm^{-2}, 365 nm) used to partially cure the LCE, as shown in Figure 1B. A Nordson 7 018 029 straight stainless-steel tip is attached to the barrel and the extrusion setup is heated to 60 °C to decrease the viscosity of the polymer so that it can be extruded. The printing bed remains at room temperature.

After the LCE is printed and cured in the custom UV chamber, a biphasic conductive ink is an extrusion printed over the actuator surface to create a Joule heater, as shown in Figure 1C. The biphasic ink is a conductive polymer (Ag-EGaIn-SIS) with high stretchability of more than 600% and conductivity of 7.02 × 10^5 S m^{-1}. Also, it is highly adhesive to substrates and exhibits only a modest gauge factor (0.9) related to the ratio of percent increase in trace resistance with mechanical strain. Prepared by mixing silver flakes and eutectic indium-gallium alloy in a styrene-isoprene-styrene polymeric matrix. The synthesis, property characterization, and printing processes for the biphasic conductor is described in ref. [52] and detailed in the Experimental Section. An example of a printed LCE actuator with an integrated Ag-EGaIn-SIS heating element is shown in Figure 1D.

Figure 2A summarizes the full LCE fabrication pipeline: First, the LCE is extruded using a heated extrusion system. This is followed by low-intensity UV curing by a flashlight (Alonefire, 365 nm, 15 W) that accompanies the printing head, as shown in Figure S1 (Supporting Information). UV exposure is needed since the LCE is still in liquid phase and a partial curing is necessary to lock the mesogens in the shear-induced aligned state. This step is especially important because effective actuation of LCEs relies on the alignment of the mesogens, which in the case of extrusion printing is induced by the shear stresses occurring in the interface surface between the LCE paste and the inner walls of the dispensing tip,[53] as shown in Figure 2A. The printed actuator is then placed inside the custom UV curing chamber (60 W, 365 nm) and finally the Joule heater is printed on the LCE surface using the biphasic stretchable conductive compound.

LCE printing is performed over a silicone substrate (Ecoflex 35) to achieve easy removal of the sample. The printed features are then irradiated in a custom UV curing chamber. The UV chamber was designed with a wavelength that matches the peak absorbance of the I369 photoinitiator – in the range of 300–350 nm[54] – as can be seen in Figure 2B.

Figure 2C compares the duration of the curing process of printed LCEs using three distinct UV irradiation systems: the custom dual-side rapid cure chamber, a conventional UVP crosslinker chamber (365 nm),[43] and a UV sterilizer chamber (250 nm). This last shows the impact that UV exposure at a

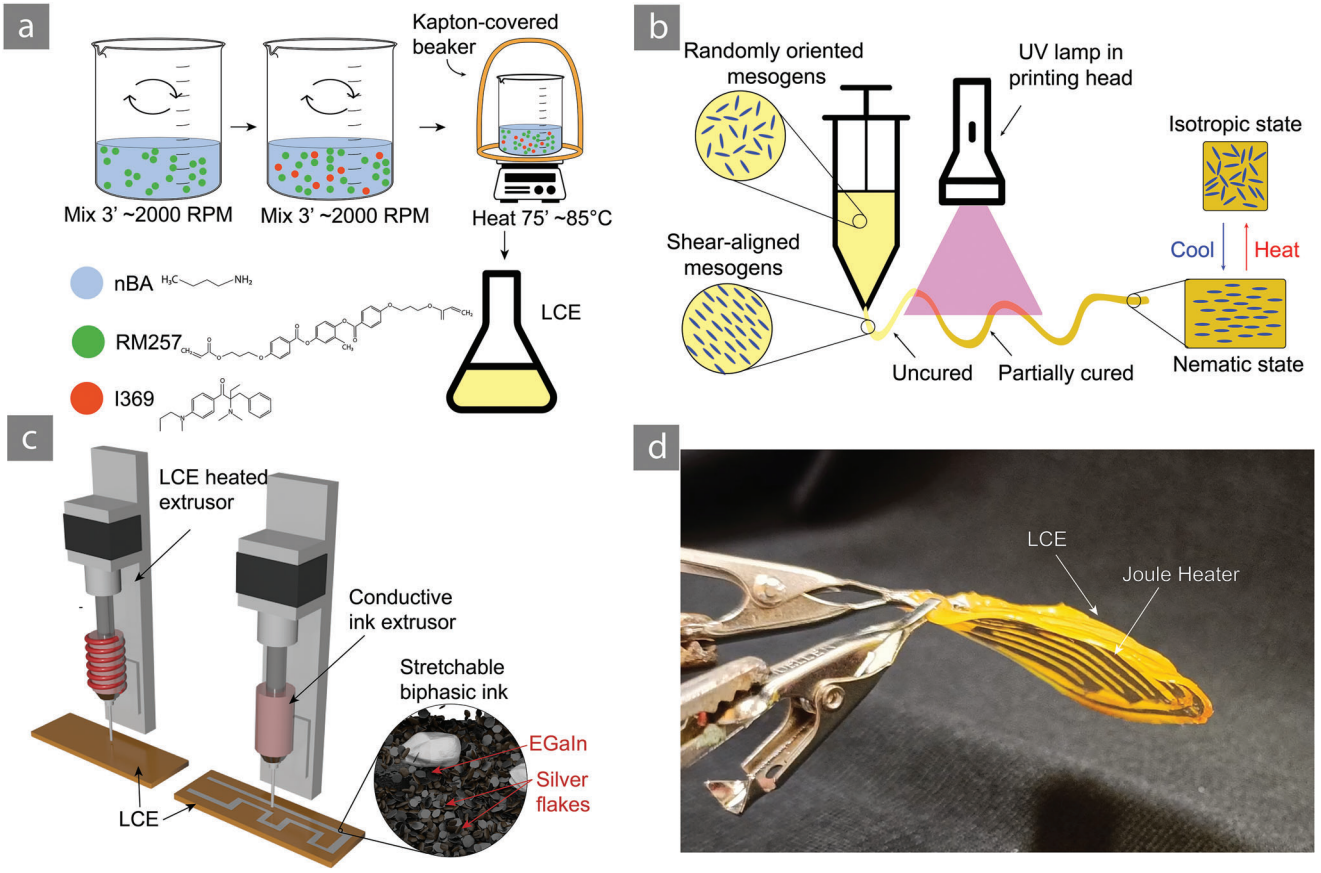

Figure 1. a) LCE synthesis procedure: Monomer, chain extender and photoinitiator mixing and polymerization by heat; b) LCE printing procedure: alignment of mesogens by sheer force and partial cure by UV light; c) LCE and conductive traces extrusion print; d) Image of circular LCE actuator by Joule heating using integrated conductive traces that are digitally printed.

wavelength that doesn't match the peak absorbance wavelength of I369 has in increasing the curing time. When comparing the chamber in ref. [43] with our work, which used the same UV wavelength, we can observe that, by increasing only the power of UV lights in 25% (60 W compared to 48 W) and creating a setup that expose all the LCE surfaces to UV, we were able to reduce the curing time to only 0.25% of the time stated in ref. [43] (90 s compared to previous 10 h).

Figure 2D shows a comparison between a single versus a double UV light curing setup, as well as color differences on LCE samples polymerized in each of the configurations presented, where a darker color corresponds to better curing. These changes in coloration due to better/deeper curing have been previously observed in other works,[55,56] but their implication in LCE should be further detailed in further studies. As can be seen the curing time was significantly reduced from several hours in previous works,[43–46] to ≈90 s. Figure 2E shows the complete custom-made UV polymerization setup.

A test was performed to assess de minimum duration of curing, as well as to evaluate the penetration depth of the UV in thick LCE samples. For this, a mold was fabricated and filled with LCE solution to a height of 10 mm, as shown in Figure S2 (Supporting Information). Once again it can be observed that while the uncured polymer presents a faint yellow color, this turns into a more saturated tone after UV exposure. After 30 s exposure, the top and bottom surfaces of the cast become darker (cured) yet the bulk of the polymer remains uncured as the UV is attenuated by the cured surfaces, making it more difficult for radiation to penetrate deeper. At 90 and 180 s exposure, the 1 cm thick sample seems already cured inside the mold. Yet, when the samples are removed from the mold and cross-sectioned, we observe that UV only penetrated up to 1.1 mm deep in the top and bottom surfaces, leaving the middle of the sample uncured, as shown by the color difference. As such, the short curing time is limited to thin LCE samples up to ≈2.2 mm thick.

To further characterize both the shear-alignment of the extrusion printed LCEs and actuation temperature of the same, simple experiments were performed. Figure S3 (Supporting Information) shows polarized optical transmission microscopy images of an LCE with two perpendicular shear aligned layers. Here it can be observed that higher birefringence occurs when the angle between sample's nematic alignment and the polarization direction is 45° (Figure S3B, Supporting Information), evidencing the occurrence of shear alignment.

From the differential scanning calorimetry plot in Figure S4 (Supporting Information), the nematic-to-isotropic transition temperature (T_{NI}) was measured as ≈60 °C. As such, when actuating the LCEs, these were heated to temperatures slightly higher

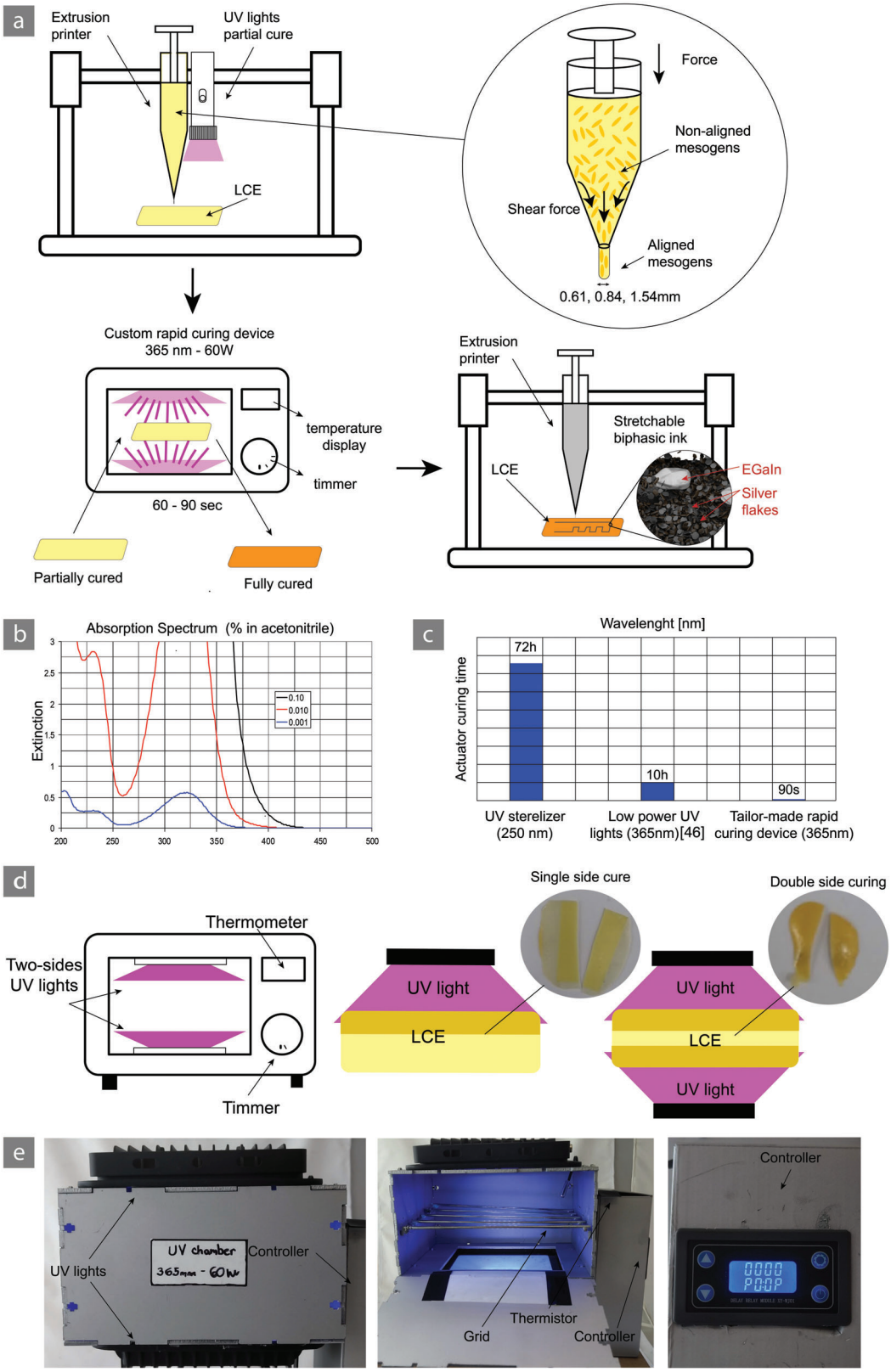

Figure 2. a) LCE fabrication pipeline. Top right inset depicts shear forces inside the extrusion barrel b) Plot depicting the optimal UV absorption spectrum for Irgacure 369 ;[54] c) Graph comparing actuator curing time for different UV exposure setups; d) Schematic comparing light setup in one and two-side curing chambers. Insets correspond to photographs of 2 different samples, one of which was cured on a single side (becoming light-colored) and the other cured on both sides (becoming darker-colored); e) Photographs of the custom dual-side UV curing chamber.

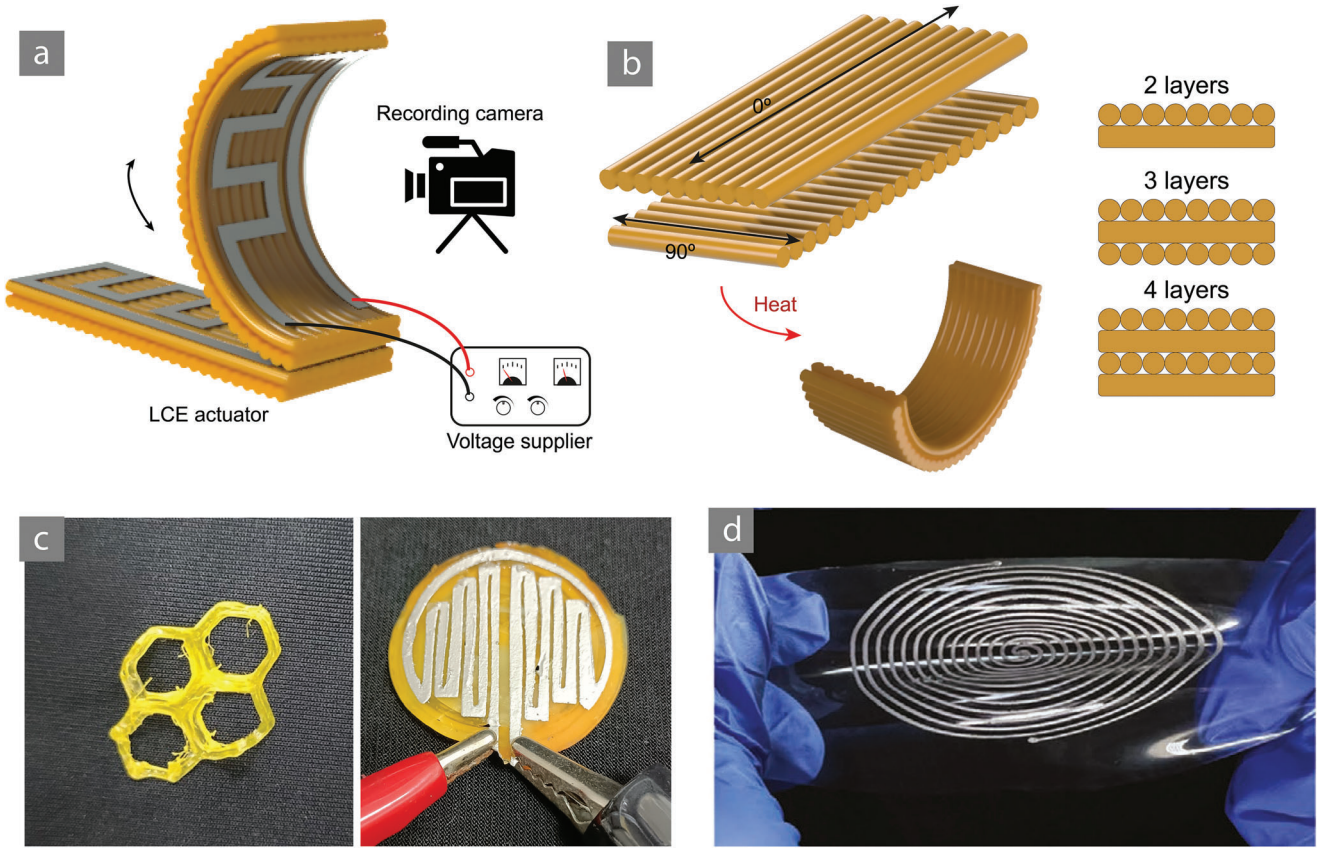

Figure 3. a) Testing setup of LCE actuator bending; b) Different geometries of rectangular LCE actuator c) Demonstrations of LCE actuators: Hexagonal and circular; d) Stretchability of biphasic conductive ink used as Joule heater printed over a TPU substrate.[60]

than the T_{NI} (i.e., ≈80 °C) to account for thermal dissipation through air and through the sample, as well as non-uniform heating of the LCE. Moreover, the small enthalpy changes corresponding to endothermic reactions in the DSC curves at the T_{NI} lead us to conclude that little energy is required to switch between nematic and isotropic states, which is advantageous in the field of actuators.

2.2. Actuator Characterization

Figure 3A shows the characterization setup used in this work, which includes the fabricated actuators, a power source, and a camera to register the bending angle of the actuators. Overall, 27 samples that vary in nozzle diameter (Φ 0.61, 0.84, and 1.54 mm), number of printed layers (2,3,4 layers), and applied voltage (1.5, 2, and 2.5 V) were studied, as can be seen in Figure 3B and Figure S5 (Supporting Information).

By employing 3D printing and direct ink writing techniques, it is possible to easily prototype and test various intricate actuator shapes, as can be seen in Figure 3C, Videos S1 and S2 (Supporting Information). These tests show both a hexagonal and a circular actuator, this last with an integrated printed Joule heater. As well, the integration of a joule heater in the honeycomb shaped LCE and its deformation after a voltage is applied are shown in Figure S6 (Supporting Information). Since the Joule heater is soft and stretchable, it can deform along with the LCE as can be seen in Figure 3D without introducing mechanical resistance to motion. This is because the heater is composed of a biphasic mixture of liquid metal alloy, silver microparticles, and soft elastomer.

Moreover, as shown in the Experimental Section and the Supporting Information file, this ink was shown to withstand high temperatures (up to 300 °C, well above the temperature needed for LCE actuation) without great impact in its electrical performance ($R/R_0 = 2$ at 60 °C and $R/R_0 = 1$ at 300 °C).

As well, from Figure S7 (Supporting Information), which shows cyclic activation of the joule heaters for 50 cycles (≈200 min), we can observe that these printed heaters can withstand long term heat exposure and are resilient to cyclic heating/cooling in the temperature range needed for LCE actuation (<≈80 °C). Moreover, it can be observed that, although most heat concentrates in the center of the heater, heat distribution is relatively even in the surrounding areas.

As shown in Figure S8 (Supporting Information), the LCE can be stretched up to 273% of its initial size before fracture and its Young modulus was estimated to be ≈11.3 MPa (averaged values for three samples) with a standard deviation of 2.012. The full strain–stress curves showing the strain at fracture and calculation of the elasticity modulus are presented in the Supporting Information.

It was observed that the actuators with three and four layers were deficient in terms of actuation since the heat delivered

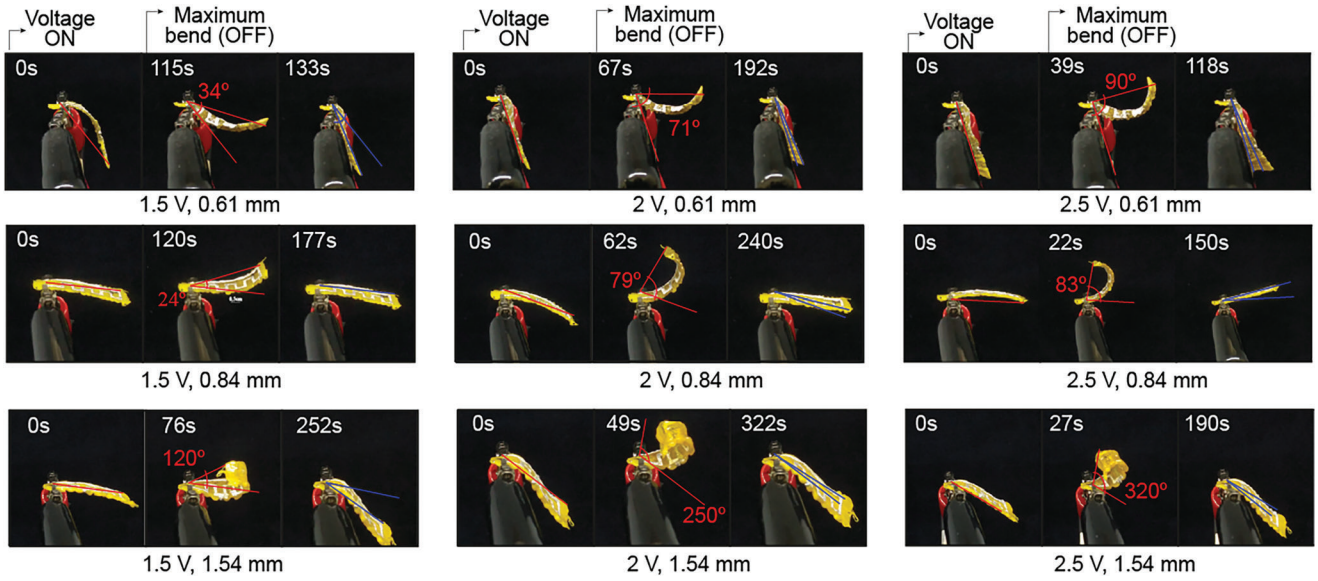

Figure 4. Images from the bending test of samples with two layers using different nozzle to print the LCE actuator. The middle panel corresponds to the maximum actuation and after this moment, the heater was turned off, so that the actuators could return to the original position, depicted in the third panel. The second panel depicts (in red) the angle between initial position. and maximum bending position. The third panel depicts (in blue) the angle between initial position and final position after the actuator cools down, showing evidence of reversible actuation."

through the printed Joule heater could not efficiently be transferred to all portions of the LCE. As shown in the Figure S9 (Supporting Information), relative to a four layer actuator, the heat is not uniformly distributed along the actuator's surface and instead seems to be concentrated in a single hot spot, which isn't observed in previous thermal images leading to a non-functional actuator. For efficient actuation of multi-layer (and consequently thicker) LCEs, it is therefore necessary to develop a more integrated Joule heater. This could be done for instance by printing the joule heater between different layers of the printed actuator, which remains a subject of future study. Nevertheless, the results of characterization for 2, 3, and 4-layer actuators are shown in Figure S5 (Supporting Information) and the extracted data is provided in Table S1 (Supporting Information). In addition, the thicker actuator results in increased stiffness, which can also contribute to lower actuation efficiency since more power would be required to induce LCE phase change and achieve deformation. Therefore, in this work, we decided to focus our in-depth analysis on actuators with two LCE layers.

Figure 4 shows images of nine samples with two printed layers that were printed using a combination of three different nozzle sizes and activated using three different levels of applied voltage. More efficient actuation (i.e., shorter time to full actuation and larger stroke) was observed in the two layer actuators when they were printed using a 1.54 mm nozzle. When printing with smaller nozzles, it is challenging to maintain printing consistency, and the print often comes with small defects. On the other hand, printing with a 1.54 mm nozzle seems sufficient for aligning the mesogens.

Referring to Figure 4, we achieved a maximum bending angle of 320° for the case where the LCE layers are printed using a 1.54 mm nozzle and the actuator is stimulated with 2.5 V. Most works in the literature do not quantify the amount of bending during the actuation.[45,57,58] Moreover, the studies that do report bending do not demonstrate angles greater than 150° or a power consumption of less than 800 mW cm^{-2}.[43,44,48,59] It's important nevertheless to note that in the case of,[43] the samples were heated by light irradiation and not by joule heating. Overall, the present work shows a significant improvement in bending performance compared to other flexural LCE actuators.

Moreover, in the figure, in each of the third panels, the angle between initial position and final position after the actuator cools down is shown (in blue), evidencing the reversibility of the actuation (that can be understood as a proof of monomer alignment). In the best cases, the reversibility angle is 0° (1.5 V, 0.84 mm), while in the worst case there is an hysteresis angle corresponding to 23° (1.5 V, 1.54 mm).

The power consumption of LCE actuator (P) was evaluated though voltage (U) and resistance (R) drained from the power supply, normalized to the entire surface area of the actuator (A), using the formula in Equation 1:

$$P = \frac{U \wedge 2}{R * A} \tag{1}$$

For this case the calculated power consumption was ≈620 mW cm^{-2}, which is an improvement compared to previous work.[43] This increase in bending angle and reduction of power consumption might be correlated with the dual sided curing chamber which can enable more complete photopolymerization and improve the alignment of the LCE mesogens. In particular, it prevents the mesogens from shifting into a disordered state due to poor curing of the deeper inner layers of the LCE, which can occur with conventional single-sided UV curing.

Video S5 (Supporting Information) shows a similar actuator to the ones depicted in Figure 4, without a printed joule heater. In this case, the LCE is actuated by a heat gun blowing hot air over the sample. During the four actuation cycles shown, reversible

actuation can be observed and it can be seen that the printed joule heater does not negatively impact actuation since some of the samples in Figure 4 (with joule heater) shown larger actuation than the one in Video S5 (Supporting Information) (without joule heater).

2.3. Demonstrations

The proposed materials and methods for soft LCE actuators permits digital fabrication of custom-made actuator designs with the desired geometry for the Joule heater. This permits greater freedom for implementation of custom-made actuators with the desired shape and bending profile. Here we present some examples of the printed actuators using the described materials and methods.

Figure 5A and Video S3 (Supporting Information) demonstrate a printed actuator that weights 46 mg and is capable of lifting and holding a weight (plastic dumbbell, 160 mg) that is approximately four times of its own weight.

Due to the versatility in design that is enabled by digital printing, it is possible to rapidly implement various geometries of the actuator and achieve different actuation profiles. For instance, as shown in Figure 5B and Video S2 (Supporting Information), we demonstrate a circular actuator that can reshape itself as a cone when voltage is applied. Also, Figure 5C shows the same behavior heated by a heating pad at its bottom. This non-conventional actuation is possible thanks to the concentric deposition of the LCE polymer during printing. Lastly, Figure 5D shows the curling actuation of a rectangular printed transducer reaching 320°. This actuator has the same geometry as the one previously shown in Figure 3B, with two layers.

3. Conclusion

In this work we demonstrated a fully digitally printed actuator produced by extrusion printing of a LCE and a biphasic stretchable ink based on a liquid metal and silver composite. This combination permitted direct digital printing of actuators with customized shape, and the desired geometry for the Joule heater circuit. Compared to other printed ink, such as Ag-based conductive composites that requires sintering at high temperatures, the LM-Ag-elastomer composite used in this work enables three advantages. First, the sinter-free printing of the Joule heater eliminates the need for heating the LCE that can damage its mechanical properties and mesogens orientation. Second, elimination of the thermal sintering enables rapid printing. Lastly, stretchability and the self-healing property of the ink permits multiple cycles of strain without losing the electrical conductivity.

In addition, we developed a custom dual-side UV curing station that enables faster curing of the LCE in ≈90 s. This contrasts with the several hours for UV curing that has been previously reported in the literature.[43–46] Moreover, this approach improves curing of the deeper layers within thicker LCE actuators. UV-mediated photopolymerization was performed by irradiating the whole surface of the LCE with high intensity UV light from both sides and using a frequency that closely matches that of the peak absorption of the photo-initiator.

Through these improvements and optimization of printing parameters, we were able to implement actuators with a large maximum bending angle of 320° and low power consumption of ≈620 mW cm^{-2} (Video S4, Supporting Information). Compared to other flexural LCE actuators, these metrics represent an improvement in actuator performance. In addition, we present fully digitally printed actuators that vary in geometry and actuation profile. Together, these demonstrations suggest that UV-mediated co-printing of LCE and biphasic conductive inks can allow for digitally printed soft actuators with a wide range of design and performance possibilities.

4. Experimental Section

LCE Synthesis: The monomer (1 g, RM257, BLD pharma) was pressed in a vial using a spatula, and the chain extender (0.124 g, butylamine, Merck) was added and mixed for 3 min at 2000 RPM in a planetary mixer (Thinky, ARE-250). Then, the photoinitiator (0.046 g, I369, BCH Brühl) was added) and the solution was again mixed. The hot bath (75 min at 85 °C) promoted oligomerization of the monomer chains so the compound could be extruded.

LCE Printing: After initial oligomerization in the hot bath, the LCE compound was transferred to the metallic extrusion barrel connected to the printer (Hydra 21, Hyrel3D) and heated to 60 °C. The piston and the nozzle were attached, and the extrusion barrel was primed, starting the ink flow. A UV flashlight (365 nm) module pointed to the nozzle was attached to the other head of the printer to lock the shear aligned LCE mesogens in place right after extruded. A paper tube was used to limit the amount of UV light directly reaching the nozzle and to prevent the LCE from being cured inside it and blocking it, as shown in Figure S10 (Supporting Information). This step was relevant since the alignment of the mesogens in this extrusion-based protocol depends on the shear forces between the mesogens and the inner walls of the dispensing tip, and, if not locked in place right after extrusion, the monomers would flow randomly, compromising actuation efficiency. During the whole printing process, the printing bed (and printing substrate) remains at room temperature.

LCE Polymerization: The custom chamber relies on two UV lamps with 365 nm wavelength and ≈2365 mW cm^{-2} power each, positioned on opposite sides of the chamber, facing inward. This disposition and power of the lamps were chosen to homogenously cure the entire surface area and deeply cure the actuator. The samples were placed inside the chamber during ≈90 s. Images of the chamber can be observed in Figure 2E.

Conductive Ink Preparation and Printing: It started by synthesizing the conductive Ag–In–Ga–SIS ink as presented.[52] First SIS (Styrene–Isoprene Copolymer – Aldrich Chemistry) was diluted in Toluene (1:3 wt.%). Silver flakes (Ag071 Technic inc.) were mixed into the SIS solution (2:1 wt.%) using a planetary mixer (Thinky ARE-250) for 3 min at 2000 rpm. Previously prepared EGaIn (75.5% Ga, 24.5% In) was mixed into the Ag-SIS solution in 2:1 EGaIn: Ag wt. % ratio and the solution was mixed in the planetary mixer for 3 min at 2000 rpm. The resulting Ag–In–Ga–SIS solution – now with a shiny silvery color – was over the surface of the actuator. The shape and dimensions of the joule heater for the rectangular actuators is shown in Figure S11 (Supporting Information). The printed ink tracks presented a width of 2 mm and a thickness (printing height) of ≈150 um. This joule heater shape was chosen since it was the one that covered the most of actuator (including the corners of rectangular samples). Nevertheless, more efficient actuator designs should be evaluated in the future.

Electromechanical and Thermal Characterization: For testing the electromechanical and actuation characteristics of the LCE transducers, samples were printed with two layers aligned perpendicular to each other, as can be seen in Figure 2A.

To perform the actuation tests and to create a dataset depicting the thermal-induced deformation in different samples. Samples with two, three and four-layers were printed, but it was observed an increase in

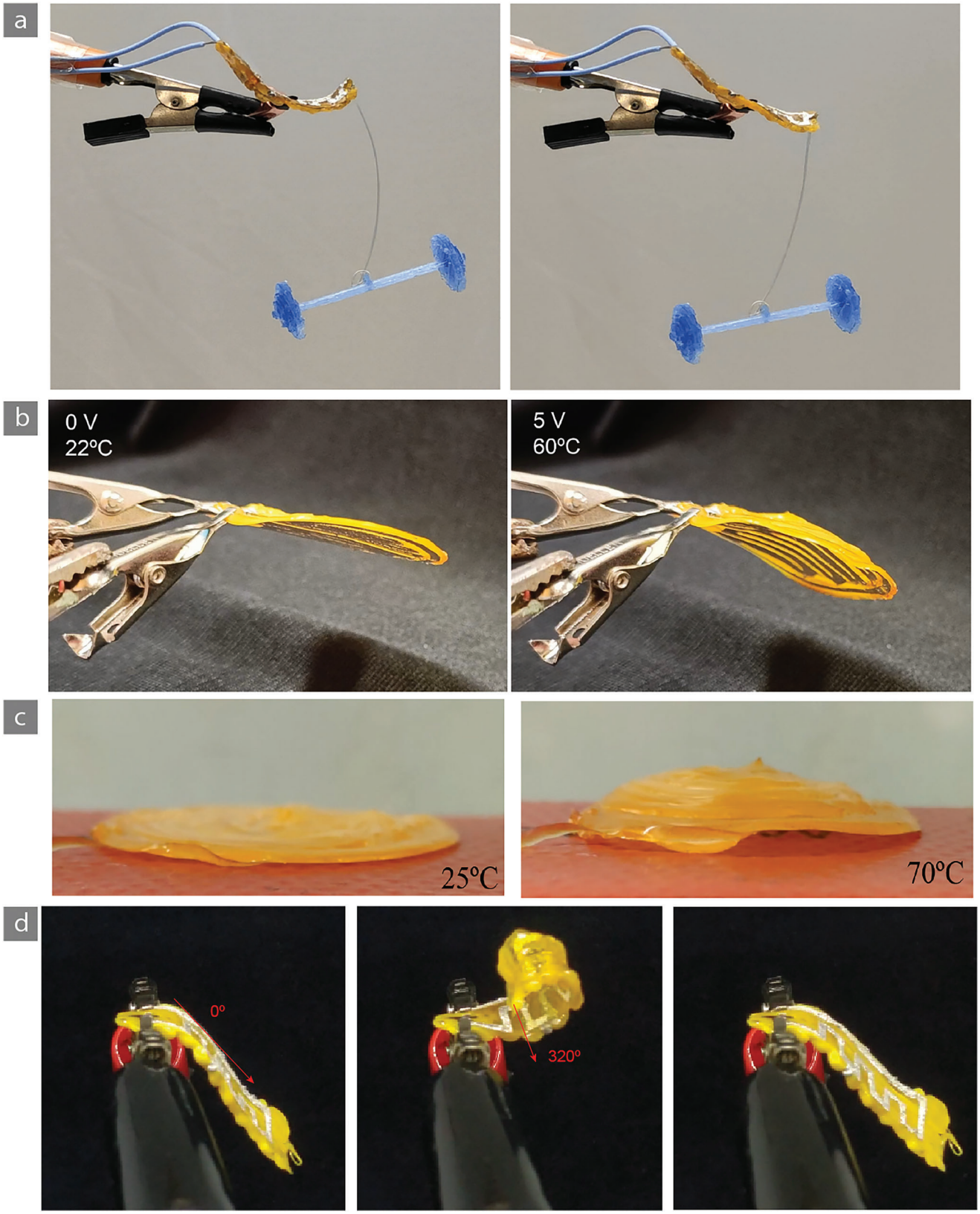

Figure 5. a) LCE actuator (0.4 g) lifting a 3D-printed barbell (1.6 g); b) Circular actuator electrically stimulated by 5 V; c) Circular actuator from side being stimulated by a heating bed until 70 °C; d) Two-layers linear actuator printed by a 1.54 mm nozzle, triggered by joule heater achieving 320° of bending.

stiffness at the three and four-layers that reduced the achievable deformation. The matrix-image with all samples is in the Figure S5 (Supporting Information) and a table where the data was extracted is in Table S1 (Supporting Information). Each LCE actuator was controlled by an electrical current delivered to the printed joule heater until maximum deformation was observed.

For testing the response of the conductive ink to temperature increase, two conductive tracks were printed over a FR-4 substrate (chosen due to its high heat resistance) and their conductivity was measured after leaving them in the oven for 15 min at different temperatures from 25 to 300 °C, as shown in Figure S12 (Supporting Information). At this temperature (300 °C) the FR-4 already reached its limit.

The temperature was measured by NTC100K thermistor, while the deformation of the actuator was recorded in video (Asus ZenFone Max M2 ZB633KL), as shown in Figure 3A. Both contraction (heating) and retraction (cooling-down) of the LCEs were recorded. Also recorded were the voltage, starting time, maximum contraction time, retraction time, contraction angle, and radius of contraction.

To determine de bending angle of each LCE sample in different temperatures, the images where the actuators were at their maximum bending were overlayed with a protractor. Considering the unactuated (resting) position as the reference (0°), the actuation angle was then measured by considering the position and orientation of the LCE's tip at maximum bending. This procedure can be seen at Figure S13 (Supporting Information).

Differential Scanning Calorimetry: Differential Scanning Calorimetry tests were performed with two UV-cured LCE samples with weights 5.8380 and 11.1728 mg (respectively the black and red lines in the plot in Figure S4, Supporting Information). DSC was performed in a mDSC calorimeter (TA instruments, Q100) between −50 and 150 °C, with a heating rate of 10 K min^{-1}.

Supporting Information

Supporting Information is available from the Wiley Online Library or from the author.

Acknowledgements

J.S.V. and M.R.C. contributed equally to this work. Support for this research was provided by the Fundação para a Ciência e a Tecnologia (Portuguese Foundation for Science and Technology) through the Carnegie Mellon Portugal Program under Grant SFRH/BD/150691/2020. Funding also came from the Carnegie Mellon Portugal Program under the project Exoskin (reference. CMU/TIC/0045/2021), and the European Union under European Research Council grant (ERC, Liquid3D, 101045072). Views and opinions expressed are however those of the author(s) only and do not necessarily reflect those of the European Union or the European Research Council. Neither the European Union nor the granting authority can be held responsible for them. The authors would like to express sincere gratitude to Professor Jorge Coelho and his research lab, Polysyc – University of Coimbra, for graciously allowing the authors to use Differential Scanning Calorimetry (DSC) equipment.

Conflict of Interest

The authors declare no conflict of interest.

Data Availability Statement

The data that support the findings of this study are available from the corresponding author upon reasonable request.;

Keywords

4D printing, direct ink printing, liquid crystal elastomer, soft actuators, soft robotics

Received: March 17, 2023
Published online:

[1] F. Iida, C. Laschi, *Procedia Comput Sci* **2011**, *7*, 99.
[2] M. Abedin-Nasab, *Handbook of Robotic and Image-Guided Surgery*, Elsevier Science Publishing Co Inc, Amsterdam, Netherlands **2019**.
[3] P. York, N. Jafferis, R. Wood, *Sens Actuators A Phys* **2020**, *311*, 112066.
[4] S. Sherrit, L. Domm, X. Bao, Y. Bar-Cohen, Z. Chang, M. Badescu, Sensors and Smart Structures Technologies for Civil, Mechanical, and Aerospace Systems 2012, SPIE, San Diego, California, USA, **2012**.
[5] S. Goetz, E. Sode, "Hpowermotion.", https://www.hpowermotion.com/product-finder (accessed December, **2021**).
[6] O. Pabst, J. Perelaer, E. Beckert, U. S. Schubert, R. Eberhardt, A. Tünnermann, *Org. Electron.* **2013**, *14*, 3423.
[7] H. Ali, S. Noor, S. M. Bashi, M. H. Marhaban, "A Review of Pneumatic Actuators (Modeling and Control) Optimal Nonlinear Model Reference Controller Design for Ball and Plate System View project," 2009. [Online]. Available: https://www.researchgate.net/publication/223260423 (accessed: January **2009**).
[8] G. K. Klute, J. M. Czerniecki, B. Hannaford, IEEE/ASME International Conference on Advanced Intelligent Mechatronics, AIM, IEEE, Atlanta, GA, USA **1999**, pp. 221–226.>
[9] F. Daerden, D. Lefeber, *Eur J Mech Env Eng.* **2002**, *47*, 11.
[10] N. Wang, B. Chen, X. Ge, X. Zhang, W. Wang, *Front. Mechan. Eng.* **2020**, *16*, 163.
[11] D. Drover, E. Hawkes, "BreathFirst Self-Guided Endo Tracheal Intubation Device A novel approach providing consistent, safe, rapid intubations".
[12] L. Ge, F. Chen, D. Wang, Y. Zhang, D. Han, T. Wang, G. Gu, *Soft Robot* **2020**, *7*, 583.
[13] D. Drotman, M. Ishida, S. Jadhav, M. T. Tolley, *IEEE ASME Trans Mechatron* **2019**, *24*, 78.
[14] E. W. Hawkes, L. H. Blumenschein, J. D. Greer, A. M. Okamura, *Sci Robot* **2017**, *2*, eaan3028.
[15] E. Hajiesmaili, D. R. Clarke, *J. Appl. Phys.* **2021**, *129*, 151102.
[16] M. Reis Carneiro, C. Majidi, M. Tavakoli, *Adv. Eng. Mater.* **2022**, *24*, 2100953.
[17] A. Chortos, E. Hajiesmaili, J. Morales, D. R. Clarke, J. A. Lewis, *Adv. Funct. Mater.* **2020**, *30*, 1907375.
[18] X. Zhang, M. Qian, In *Magnetic Shape Memory Alloys*, 1st ed., Springer, Singapore, **2022**.
[19] N. A. Meisel, A. M. Elliott, C. B. Williams, *J Intell Mater Syst Struct* **2015**, *26*, 1498.
[20] D. J. Hartl, D. C. Lagoudas, *Proc Inst Mech Eng G J Aerosp Eng* **2007**, *221*, 535.
[21] K. Hu, K. Rabenorosoa, M. Ouisse, *Front Robot AI* **2021**, *8*, 678486.
[22] M. H. Mat Yazik, M. T. H. Sultan, *Failure Analysis in Biocomposites, Fibre-Reinforced Composites and Hybrid Composites*, Woodhead Publishing, United Kingdom, **2019**, pp. 181–198.
[23] G. Ehrmann, A. Ehrmann, *J. Appl. Polym. Sci.* **2021**, *138*, 50847.
[24] T. Xie, *Polymer* **2011**, *52*, 4985.
[25] R. S. Kularatne, H. Kim, J. M. Boothby, T. H. Ware, *J Polym Sci B Polym Phys* **2017**, *55*, 395.
[26] Q. He, Z. Wang, Y. Wang, A. Minori, M. T. Tolley, S. Cai, *Sci. Adv.* **2019**, *5*, eaax5746.
[27] Z. Pei, Y. Yang, Q. Chen, E. M. Terentjev, Y. Wei, Y. Ji, *Nat. Mater.* **2014**, *13*, 36.
[28] M. Shahinpoor, *Smart Structures and Materials 2000: Electroactive Polymer Actuators and Devices (EAPAD)*, Vol. *3987*, SPIE, Bellingham, WA, **2000**, p. 187.
[29] T. A. Kent, M. J. Ford, E. J. Markvicka, C. Majidi, *Multifunctional Materials* **2020**, *3*, 025003.

[30] M. Barnes, S. M. Sajadi, S. Parekh, M. M. Rahman, P. M. Ajayan, R. Verduzco, *ACS Appl. Mater. Interfaces* **2020**, *12*, 28692.
[31] Z. Wang, Z. Wang, Y. Zheng, Q. He, Y. Wang, S. Cai, *Sci Adv.* **2020**, *6*, eabc0034.
[32] M. Del Pozo, J. A. H. P. Sol, A. P. H. J. Schenning, M. G. Debije, *Adv. Mater.* **2022**, *34*, 2104390.
[33] T. J. White, D. J. Broer, *Nat. Mater.* **2015**, *14*, 1087.
[34] M. Shahinpoor, *Smart Structures and Materials 2000: Electroactive Polymer Actuators and Devices (EAPAD)*, Vol. *3987*, SPIE, Bellingham, WA, **2000**, p. 187.
[35] G. E. Bauman, J. D. Hoang, M. F. Toney, T. J. White, *ACS Macro Lett.* **2023**, *12*, 248.
[36] C. P. Ambulo, J. J. Burroughs, J. M. Boothby, H. Kim, M. R. Shankar, T. H. Ware, *ACS Appl. Mater. Interfaces* **2017**, *9*, 37332.
[37] K. M. Herbert, H. E. Fowler, J. M. Mccracken, K. R. Schlafmann, J. A. Koch, T. J. White, *Nat. Rev. Mater.* **2022**, *7*, 23.
[38] G. E. Bauman, J. M. Mccracken, T. J. White, *Angew. Chem. – Int. Ed.* **2022**, *61*, e202202577.
[39] J. W. Boley, W. M. Van Rees, C. Lissandrello, M. N. Horenstein, R. L. Truby, A. Kotikian, J. A. Lewis, L. Mahadevan, *Proc Natl Acad Sci U.S.A* **2019**, *116*, 20856.
[40] J. Sun, Y. Wang, W. Liao, Z. Yang, *Small* **2021**, *17*, 2103700.
[41] Z. Wang, H. Tian, Q. He, S. Cai, *ACS Appl. Mater. Interfaces* **2017**, *9*, 33119.
[42] Q. He, Z. Wang, Y. Wang, A. Minori, M. T. Tolley, S. Cai, *Sci. Adv.* **2019**, *5*, eaax5746.
[43] C. P. Ambulo, M. J. Ford, K. Searles, C. Majidi, T. H. Ware, *ACS Appl. Mater. Interfaces* **2021**, *13*, 12805.
[44] Y. Wang, J. Liu, S. Yang, *Appl. Phys. Rev.* **2022**, *9*, 011301.
[45] M. Barnes, R. Verduzco, *Soft Matter* **2019**, *15*, 870.
[46] B. Zuo, M. Wang, B.-P. Lin, H. Yang, *Nat. Commun.* **2019**, *10*, 4359.
[47] C. Wang, K. Sim, J. Chen, H. Kim, Z. Rao, Y. Li, W. Chen, J. Song, R. Verduzco, C. Yu, *Adv. Mater.* **2018**, *30*, 1706695.
[48] M. Wang, Z.-W. Cheng, B.o Zuo, X.u-M. Chen, S. Huang, H. Yang, *ACS Macro Lett.* **2020**, *9*, 860.
[49] M. D. Dickey, R. C. Chiechi, R. J. Larsen, E. A. Weiss, D. A. Weitz, G. M. Whitesides, *Adv. Funct. Mater.* **2008**, *18*, 1097.
[50] X. Yu, W. Fan, Y. Liu, K. Dong, S. Wang, W. Chen, Y. Zhang, L. Lu, H. Liu, Y. Zhang, *Adv. Mater. Technol.* **2022**, *7*, 2101618.
[51] M. Tavakoli, P. Alhais Lopes, A. Hajalilou, A. F. Silva, M. Reis Carneiro, J. Carvalheiro, J. Marques Pereira, A. T. De Almeida, *Adv. Mater.* **2022**, *34*, 2203266.
[52] A. Hajalilou, A. F. Silva, P. A. Lopes, E. Parvini, C. Majidi, M. Tavakoli, *Adv. Mater. Interfaces* **2022**, *9*, 2101913.
[53] S. Wenhui, C. Shouxi, J. Yongze, Q. Renyuan, *Liquid Crystals Reviews*, vol. *19*, Taylor and Francis Ltd., Oxfordshire, USA, **2007**, pp. 549–555.
[54] Ciba Specialty Chemicals, "Irgacure 369." http://www.xtgchem.cn/upload/20110629045432.PDF (accessed November 20, **2022**).
[55] D. S. Kumar, M. J. Shukla, K. K. Mahato, D. K. Rathore, R. K. Prusty, B. C. Ray, in *IOP Conference Series: Materials Science and Engineering*, Vol. *75*, IOP Publishing Ltd., Bristol, UK, **2015**.
[56] D. Kim, J. i-S. Shim, D. Lee, S.-H. o. Shin, N. a-E. Nam, K.-H. Park, J.-S. Shim, J.-E. Kim, *Polymers* **2020**, *12*, 2762.
[57] C. Ohm, M. Brehmer, R. Zentel, *Adv. Mater.* **2010**, *22*, 3366.
[58] S. W. Ula, N. A. Traugutt, R. H. Volpe, R. R. Patel, K. Yu, C. M. Yakacki, *Liquid Crystals Reviews*, Vol. *6*, Taylor and Francis Ltd., Oxfordshire, USA, **2018**.
[59] D. Sun, J. Zhang, H. Li, Z. Shi, Q.i Meng, S. Liu, J. Chen, X. Liu, *Polymers* **2021**, *13*, 1889.
[60] W. Zu, Y. Ohm, M. R. Carneiro, M. Vinciguerra, M. Tavakoli, C. Majidi, *Adv. Mater. Technol.* **2022**, *7*, 2200534.